Estuarine, Coastal and Shelf Science 315 (2025) 109155

Contents lists available at ScienceDirect

Estuarine, Coastal and Shelf Science

journal homepage: www.elsevier.com/locate/ecss

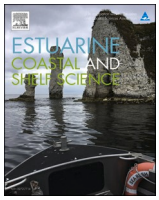

Wave attenuation over a *Scirpus mariqueter* salt marsh during typhoon Muifa

Ming Shi [a], Zhijun Dai [a,b,*], Jiejun Luo [a], Jie Wang [a], Wenhong Pang [c], Xixing Liang [c], Jinping Cheng [d]

[a] State Key Laboratory of Estuarine and Coastal Research, East China Normal University, Shanghai, 200241, China
[b] Laboratory for Marine Geology, Qingdao Marine Science and Technology Center, Qingdao, 266061, China
[c] Guangxi Key Laboratory of Marine Environmental Change and Disaster in Beibu Gulf, Beibu Gulf University, Qinzhou, 200062, China
[d] Department of Science and Environmental Studies, The Education University of Hong Kong, New Territories, Hong Kong, China

ARTICLE INFO

Keywords:
Scirpus mariqueter
Salt marsh
Typhoon muifa
Drag coefficient
Wave attenuation

ABSTRACT

Salt marshes play a crucial role in mitigating coastal flooding by wave attenuation. However, widespread degradation of these natural barriers due to human activities has exacerbated the hazards associated with large waves during typhoon events. This study presents field observations of wave dynamics and salt marsh characteristics conducted in Chongming Dongtan, located in the Changjiang estuary, in September 2022 under varying weather conditions. The objective was to investigate wave variations over the *Scirpus mariqueter* salt marsh. The results show that the average wave attenuation during Typhoon Muifa was 6% lower than that under normal wave conditions. Additionally, the maximum significant wave height experienced a 19% reduction in attenuation during Muifa compared to normal wave conditions. Insufficient wave attenuation was attributed to deeper water depths. Furthermore, the drag coefficient was lower during typhoon events, likely due to prolonged inundation durations and larger vertical gaps between the water surface and the top of the *Scirpus mariqueter*. This study highlights the important role of *Scirpus mariqueter* in dissipating waves during typhoon events and provides a theoretical basis for wetland conservation and coastal ecological security.

1. Introduction

Salt marshes are highly valuable ecosystems that act as natural buffers against storms at the land–sea interface, provide habitats for intertidal species, and offer significant economic and recreational benefits to humans (Mariotti and Fagherazzi, 2010). However, rising sea levels and intensified storm surges due to global warming have led to significant losses of salt marsh wetlands (Kirwan and Megonigal, 2013). Typhoons not only cause severe erosion in salt marshes but also result in permanent structural damage to these ecosystems (Leonardi, 2021). The frequency of typhoons impacting East and Southeast Asia has increased by 12–15% over the past 40 years, further accelerating the degradtion of tidal flats (Deegan et al., 2012; Mei and Xie, 2016).

Salt marshes naturally attenuate wave energy, and their loss amplifies the risk of inundation from typhoon-induced waves in coastal areas (Kearney and Stevenson, 1991; Jadhav et al., 2013; Möller et al., 2014; Stark et al., 2015; Gracia et al., 2018; Nordio and Fagherazzi, 2022). For instance, wave attenuation rates of 0.63% per meter have been recorded over *Spartina alterniflora* salt marsh (Paquier et al., 2017), which increased to 1.49 %/m with larger incident waves (Zhang et al., 2020a). The wave attenuation rate along mangroves is around 0.50 %/m (Zhang et al., 2022b), while the Bulrush salt marsh demonstrated an attenuation rate of 1.31 %/m (Zhang et al., 2022a). Understanding wave propagation over salt marshes during typhoons is essential for developing effective coastal defense strategies through ecological engineering (Zhang et al., 2022a).

Several studies utilizing field observations (Jadhav et al., 2013), laboratory experiments (Augustin et al., 2013; Xu et al., 2022), and numerical simulations (Smith et al., 2016) have demonstrated the significant impact of vegetation on wave attenuation, specifically regarding how salt marshes mitigate wave energy generated by typhoons. During wave propagation, salt marshes enhance turbulent energy dissipation (Temmerman et al., 2013) and facilitate the transformation of wave energy into potential energy (Möller et al., 1999, 2014; Van Loon-Steensma, 2015). Vegetation disrupts water flow, resulting in reduced flow velocity and wave height(Van Proosdij et al.,

* Corresponding author. State Key Laboratory of Estuarine and Coastal Research, East China Normal University, Shanghai, 200241, China.
E-mail address: zjdai@sklec.ecnu.edu.cn (Z. Dai).

https://doi.org/10.1016/j.ecss.2025.109155
Received 30 March 2024; Received in revised form 25 December 2024; Accepted 24 January 2025
Available online 28 January 2025

2000, 2006). Furthermore, salt marshes have been shown be more effective in wave dissipating during typhoon events compared to normal wave conditions (Temmerman et al., 2005; Neumeier and Amos, 2006).

The effectiveness of salt marshes in wave attenuation is influenced by various vegetation characteristics (Paul et al., 2012; Mendez and Losada, 2004; Spencer et al., 2016; Marsooli et al., 2017; Willemsen et al., 2020). Specifically, salt marsh stems with higher stiffness tend to oscillate during wave cycles (Luhar et al., 2010). However, these flexible stems can bend at larger angles, forming a protective layer over the seabed that may reduce their effectiveness in damping water flow (Paul et al., 2016). Moreover, the movement of vegetation stems leads to decreased wave attenuation as wave energy increases (Bouma et al., 2005; Riffe et al., 2011). While rigid vegetation may provide superior wave attenuation (Silinski et al., 2015), it is also more susceptible to breakage under intensive hydrodynamic forces (Puijalon et al., 2011; Heuner et al., 2017).

Most existing studies have primarily investigated changes in wave attenuation in salt marsh vegetation through laboratory experiments and numerical simulations (Chen and Zhao, 2012; Chong et al., 2021; Ma et al., 2023). However, laboratory experiments often face spatial constrains, and the results obtained from the numerical simulations can lack realism (Beena et al., 2019; Garzon et al., 2019). Moreover, field observations have predominantly focused on wave attenuation under normal conditions, largely due to challenges in data collection during extreme weather events (Mazda et al., 2006; Jadhav et al., 2013).

While substantial research has been dedicated to wave attenuation in salt marshes (Zhou et al., 2022; Wei et al., 2022), few studies have specifically investigated wave propagation in *Scirpus mariqueter* salt marshes, particularly under extreme weather conditions. *Scirpus mariqueter*, as a native vegetation species in China, plays an important role in wave attenuation within the salt marsh of Chongming Dongtan in the Changjiang estuary. Therefore, the present study aimed to deploy an instrumented transect with four stations across the *Scirpus mariqueter* salt marsh in Dongtan to analyze wave attenuation. This study aims to deploy an instrumented transect with four stations across the Scirpus mariqueter salt marsh in Dongtan to analyze wave attenuation. The primary objectives are to: 1) explore the wave attenuation process over the Scirpus mariqueter salt marsh under both normal conditions and during typhoon events, and 2) identify potential factors influencing wave attenuation in this ecosystem. This research is crucial for understanding wave propagation dynamics within Scirpus mariqueter salt marshes in estuarine regions and their role in mitigating wave impacts.

2. Methods

2.1. Study area

Dongtan, located in the Changjiang estuary, is the world's largest alluvial island (Fig. 1B). This region has experienced significant economic losses due to the impacts of large waves generated by typhoons (Zhang et al., 2020b). Covering approximately 1267 km^2, Dongtan accounts for approximately 20% of Shanghai's land area. The extensive intertidal zone spans 5.1 km in width from north to south and 10.8 km in length from east to west, covering roughly 42 km^2 (Mi et al., 2022). The salt marshes in this area are predominantly composed of clay with a grain size of 15 μm, while the mudflat primarily consist of clay with a grain size of 35 μm (Gorenc et al., 2004). Internal tides observed around Chongming Island exhibit irregular semidiurnal patterns, with wave height decreasing progressively from the entrance towards the interior, ranging from 0.4 m to 0.9 m (Lou et al., 2022). The intertidal zone of Dongtan supports a diverse array of salt marsh species, including *Bulrush*, *Scirpus mariqueter*, and *Spartina alterniflora* (Yang et al., 2008). *Scirpus mariqueter,* a native species characterized by three leaves, is widely distributed in the northern region of Chongming Island and plays a vital role in attenuating wave energy, thereby enhancing the island's resilience.

2.2. Typhoon muifa

Severe Typhoon Muifa (No. 2212) originated in the northwest Pacific Ocean on September 8, 2022, with a center wind speed of 18 m/s. It moved north by west at a speed of 10–15 km/h. Muifa made its initial landfall in Zhoushan at 20:30 on September 14, reaching a maximum center wind speed of 42 m/s. It made a second landfall at 0:30 on September 15 on the coast of Fengxian, Shanghai, with a wind speed of 35 m/s and a forward motion of 20–25 km/h (Fig. 1A). Chongming Island was affected by Typhoon Muifa from September 13 to 15, coinciding with a middle tide period. Wind intensity peaked at 30 m/s, and total precipitation ranged from 100 mm to 200 mm.

2.3. Field observation

A transect with a slope of 0.004 was set up on the tidal flat in the northern salt marsh of Chongming from September 7 to 17, 2022, approximately 630 m from the seawall (Fig. 1D). Wave breaking was not

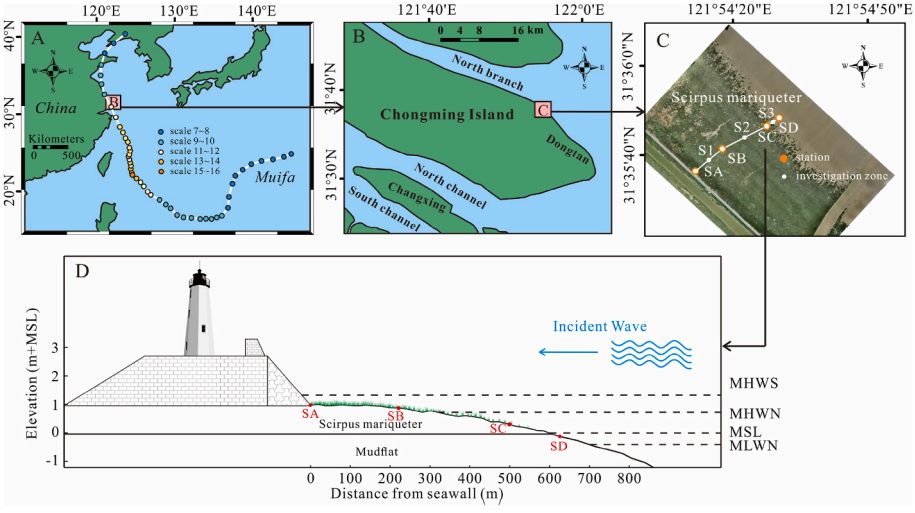

Fig. 1. (A) Map of Chongming Dongtan with its location in relation to China and typhoon path, (B) study area in relation to Chongming Island, North branch, North channel and Changxing Island, (C) stations on the *Scirpus mariqueter* tidal flat, (D) elevation in relation to the mean sea level (MSL) of the cross-shore transects with relative distance from seawall. Tidal water levels are indicated on the right axis (MHWS, mean high water level at spring tide; MHWN, mean high water level at neap tide; MLWN, mean low water level at neap tide).

considered in this study (Möller et al., 2014). This study involved four fixed observation stations to collect data on wave characteristics, water depth, and vegetation during both lunar tides and Typhoon Muifa. The four stations were positioned perpendicular to the seawall (Fig. 1C) at specific locations within the marsh ecosystem: SA (121° 54′ 11″ E, 31° 35′ 36″ N) represented the inner marsh, SB (121° 54′ 17″ E, 31° 35′ 41″ N) represented the marsh center, SC (121° 54′ 28″ E, 31° 35′ 46″ N) represented the marsh edge, and SD (121° 54′ 30″ E, 31° 35′ 48″ N) represented the marsh front. The linear distance from the coast to the stations (SA, SB, SC, SD) were 0 m, 221m, 513m, and 626m, respectively (Fig. 1D). To measure water depth, a depth logger (T-wave) and a tide and wave recorder (RBR-SOLO^3) were installed approximately 10 cm above the mud surface (Fig. 2). Wave measurements were conducted in bursts of a 15-30-min duration to adequately capture wave characteristics (Holthuijsen, 2007). Given the battery and storage capacity of the instrument, total pressure was recorded continuously at a frequency of 4 Hz, capturing data for 512s every 30 min. In addition to wave and water depth measurements, seven investigation zones (SA, S1, SB, S2, SC, S3, SD) were selected along the transect to quantify vegetation parameters. Four zones were located near the established stations, while three zones were positioned between adjacent stations (Fig. 1C). The seven measurement areas were distributed seaward, perpendicular to the shoreline, with each zone encompassing an area of 1m × 1 m. To facilitate measurement, each zone was divided into four sections. Within each zone, vegetation height was measured 4 times, and density of vegetation was assessed 2 times. The relatively uniform vegetation within the measurement areas allowed for an accurate representation of the vegetation conditions in the study area.

2.4. Wave attenuation calculation

The wave height was calculated from the pressure energy spectrum $S_p(f)$ using a fast Fourier transform considering 2048 components with 30-min windows. Then the pressure energy spectrum was converted into the water surface elevation spectrum $S_s(f)$ using linear wave theory.

$$S_s(f) = \left\{ \frac{\cosh(kd)}{\cosh[k(z+d)]} \right\}^2 S_p(f) \tag{1}$$

Where k is the wavenumber ($k = 2\pi/L$, L is the wavelength), f is the frequency, z is the depth at which the sensor is located, d is water depth.

m_0 is the variance of the one-dimensional water surface elevation spectrum $S_s(f)$

$$m_n = \int_0^\infty f^n S_s(f) \mathrm{d}f (n = 0, 1, 2, 3, 4) \tag{2}$$

Thus, the significant wave height (Hs) was calculated as

$$Hs = 4.04\sqrt{m_0} \tag{3}$$

Wave attenuation models were initially applied widely in deep-sea environments. With advancements in technology and theoretical understanding, these models have increasingly been utilized in tidal flats (Möller et al., 1999; Foster-Martinez et al., 2018). Although wave propagation is directional in both shallow and deep-water conditions, it approaches tidal flats nearly perpendicular to the shoreline (Latapy et al., 2019). In this study, the profile was arranged perpendicular to the shoreline to align with the direction of wave propagation The wave energy attenuation model takes into account factors such as refraction, attenuation, and breakage that occur during wave propagation, allowing for the calculation o wave energy attenuation (Kobayashi et al., 1993; Möller et al., 1999). Equations (1)–(3), proposed by Battjes and Janssen (1978) were used to calculate wave height and energy attenuation:

$$E = E_K + E_P = \frac{1}{8}\rho g H^2 \tag{4}$$

$$r1 = \frac{\Delta H}{H}\frac{1}{\Delta x} \tag{5}$$

$$r2 = \frac{\Delta E}{E}\frac{1}{\Delta x} \tag{6}$$

where E is the wave energy, E_K is the wave kinetic energy, E_P is the wave energy potential energy, ρ is the density of seawater, g is the acceleration of gravity, and H is the wave height. $r1$ is the wave height attenuation rate, m^{-1}, $r2$ is the wave energy attenuation rate, $J{\cdot}m^{-1}$, H is the wave height of SD; ΔH is the wave height difference between two stations; E is the wave energy of SD, ΔE is the difference in wave energy between two stations, and Δx is the distance between two points.

2.5. Calculation of drag coefficient

Based on Bretschneider's bottom friction formula for wave attenuation in shallow water without vegetation, a resistance coefficient can be obtained, which can be applied to the entire nearshore water depth region. This formula is used to estimate the resistance coefficient. The attenuation caused by bottom friction in shallow water can be obtained by Bretschneider et al. (1954):

$$\frac{H_2}{H_1} = \frac{1}{1 + \frac{\pi^5 K_s^2}{\sqrt{2}g^2 T^4} C_D H_1 \Delta x \left(\sinh\frac{2\pi h}{L}\right)^{-3}} \tag{7}$$

where H_1 and H_2 are the wave heights of SD and SA, respectively, and Δx is the distance between two observation points. h is the average water depth between two observation points, T is the wave period, L is the wavelength, g is the gravitational acceleration, K_s is the shallow water coefficient, C_D is connected with bottom shear force τ, and the relationship of C_D and τ can be defined as:

$$\tau = \frac{1}{2} C_D \rho u^2 \tag{8}$$

where ρ is the density of seawater and u is the current velocity in the direction of wave propagating. Although the above formulas were often used on the tidal flat without vegetation, they were also adapted to the

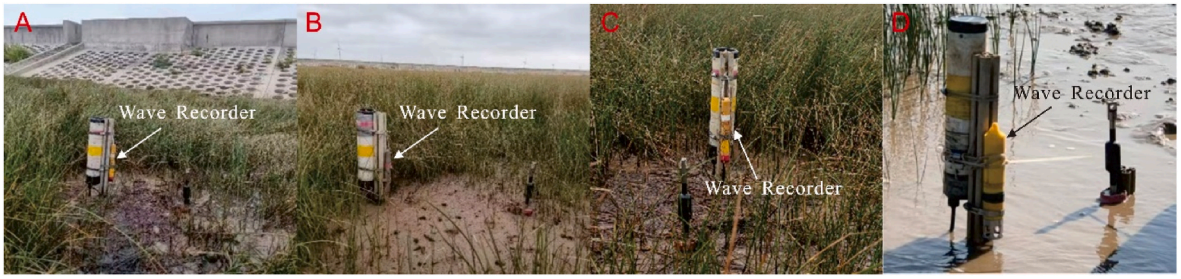

Fig. 2. The instrument placement, which includes (A) RBR-SOLO^3 at the inner marsh (SA), (B) T-wave at the marsh center (SB), (C) RBR-SOLO^3 at the marsh edge (SC), and (D) T-wave at the marsh front (SD).

salt marsh with the development of the subject (Bryant, 1979; Young and Gorman (1995); Zhou et al., 2022). Just as Mazda et al. (1997) proposed the following:

$$\frac{H_2}{H_1}=\frac{1}{1+\frac{C_D \pi H_1 \Delta x}{32\sqrt{2}h^2}} \tag{9}$$

Therefore, the resistance coefficient C_D can be derived from Equation (10):

$$C_D=\frac{32\sqrt{2}}{\pi}\frac{h^2}{H_1 \Delta x}\left(\frac{H_1}{H_2}-1\right) \tag{10}$$

3. Results

3.1. Spatial variation in Scirpus mariqueter density and height

In the present study, the transect spanning a 600 m-wide *Scirpus mariqueter* salt marsh and a 30 m-wide mudflat was established from station SA to station SD (Fig. 1D). The average density of *Scirpus mariqueter* ranged from 0 stems/m^2 at SD to 2080 stems/m^2 at SA (Fig. 3). In contrast to the vegetation density, the vegetation height initially decreased before increasing within the salt marsh, with heights recorded ranging from 0 m to 0.66 m (Fig. 3). Station SD, located in the lower tidal flat, exhibited no vegetation. Station S3 featured *Scirpus mariqueter* vegetation with an average height of 0.57 ± 0.10 m and a density of 416 ± 80 stems/m^2. Station SC displayed a distribution of *Scirpus mariqueter* with an average density of 1136 ± 208 stems/m^2 and an average height of 0.66 ± 0.07 m. At station S2, *the vegetation height was* 0.49 ± 0.05 m, with a density of 1792 ± 240 stems/m^2. As waves propagated from station SB towards station SA, the vegetation density increased from 1856 ± 288 stems/m^2 to 2080 ± 208 stems/m^2 and the height of these marshes rose from 0.36 ± 0.05 m to 0.56 ± 0.05 m. At site S1, the *average density of Scirpus mariqueter* was 1888 ± 256 stems/m^2, with a corresponding height of 0.41 ± 0.06 m.

3.2. Impact of typhoon muifa on water depth and wave characteristics

During normal wave conditions, the maximum water depth exhibited a gradual decrease from 1.68 m to 0.55 m landward (Table 1). In contrast, during Typhoon Muifa, characterized by a central air pressure below 98 kPa and landfall in Dongtan at mid-tide, the maximum water depth significantly increased. Specifically, the maximum water depth notably increased from 1.68 m to 1.84 m at site SD, from 1.44 m to 1.59 m at site SC, from 0.66 m to 0.86 m at site SB, and from 0.55 m to 0.77 m at site SA. Similarly, the average water depth also increased due to the impact of Typhoon Muifa, with values rising from 0.63 m to 0.82 m at site SD, from 0.53 m to 0.66 m at site SC, from 0.25 m to 0.30 m at site SB, and from 0.25 m to 0.30 m at site SA.

Moreover, the duration of the tide exhibited a similar trend to that of wave height. Under normal wave conditions, the average tide duration at SA, SB, SC and SD was 3.00 h, 3.50 h, 4.85 h, and 5.14 h, respectively. Typhoon Muifa extended the tide duration, resulting in average tide duration of 3.25 h, 4.20 h, 5.75 h and 6.17 h at SA, SB, SC and SD, respectively (Table 1). Significant attenuations in both maximum and average wave height (Hs) and energy (E) were observed along the transect during different periods (Table 1). During Typhoon Muifa, maximum Hs and E experienced attenuation of 80% and 95%, respectively, from SD to SA, with maximum values recorded at SD of approximately 0.71 m for Hs and 624.60 J/m^2 for E. Similarly, average Hs and E decreased by 92% and 99%, respectively, from SD to SA. In contrast, under normal conditions, maximum Hs and E showed attenuation of 99% and 100%, respectively, from SD to SA, with higher values recorded at SD—around 0.34 m for Hs and 146 J/m^2 for E. Similarly, average Hs and E attenuated by 98% and 100%, respectively, from SD to SA.

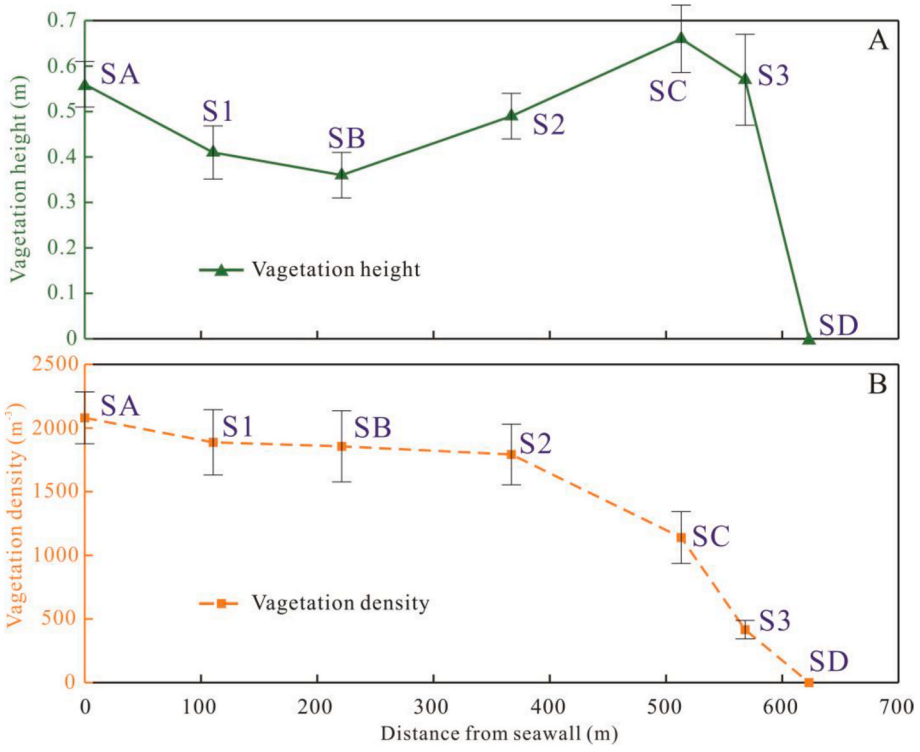

Fig. 3. Distribution of *Scirpus mariqueter* along the transect. (A) Green line is the height of vegetation of each investigation zone. (B) Yellow line is the density of vegetation of each investigation zone. The Error bars exhibit the error measurement of vegetation height. "SA" "SB" "SC" and "SD" represent the stations of inner marsh, marsh center, marsh edge and marsh front, respectively. "S1" "S2" and "S3" represent the stations between inner marsh, marsh center, marsh edge and marsh front, respectively.

Table 1
The hydrodynamic change along the transect, *h* exhibits the water depth during different period, *Hs* represents the significant wave height during different periods, and *E* displays the significant wave energy during different period.

Date	Point	Tide duration (h)	Inundation duration (h)	*h* (m)		*Hs* (m)		*E* (J/m^{-2})	
				Ave.	Max.	Ave.	Max.	Ave.	Max.
Normal wave	a	3.00	0	0.25	0.55	0.00	0.00	0.01	0.01
	b	3.50	0.50	0.25	0.66	0.00	0.01	0.01	0.12
	c	4.85	1.58	0.53	1.44	0.03	0.16	0.81	33.00
	d	5.14	2.27	0.63	1.68	0.11	0.34	13.97	146.06
Spring tide	a	2.33	0.21	0.26	0.55	0.00	0.00	0.01	0.01
	b	3.75	0.70	0.27	0.66	0.00	0.01	0.01	0.12
	c	5.33	2.41	0.69	1.44	0.04	0.16	2.00	33.00
	d	5.42	3.25	0.86	1.68	0.14	0.34	25.64	146.06
Muifa	a	3.25	0.50	0.30	0.77	0.02	0.15	0.63	27.06
	b	4.20	1.20	0.30	0.86	0.03	0.17	0.92	35.42
	c	5.75	2.83	0.66	1.59	0.13	0.52	19.23	336.62
	d	6.17	3.58	0.82	1.84	0.27	0.71	91.37	624.65

3.3. Attenuation rates of wave height and energy under varying conditions

The wave propagation from station SD to station SA exhibited distinct attenuation rates for wave height (*r1*) and wave energy (*r2*). Under normal wave conditions, the average significant wave height *Hs* at different stations revealed attenuation rates of r1 = 1.57×10^{-3} per meter and *r2* = 1.60×10^{-3} per meter from SD to SA (Fig. 5A and B). In contrast, during Typhoon Muifa, the attenuation rates were *r1* = 1.463×10^{-3} per meter and *r2* = 1.581×10^{-3} per meter. Notably, the attenuation rates under normal wave conditions were 1.07 times greater for r1 and 1.01 times greater for r2 compared to those observed during Typhoon Muifa.

Similarly, during peak spring tide, the average *Hs* at different stations exhibited attenuation rates of *r1* = 1.59×10^{-3} m^{-1} and *r2* = 1.61×10^{-3} m^{-1} from SD to SA (Fig. 5C and D). However, during peak storm surge, the attenuation rates decreased to *r1* = 1.30×10^{-3} per meter and *r2* = 1.55×10^{-3} per meter, from SD to SA. Consequently, the attenuation rates during peak spring tide were 1.23 times greater for *r1* and 1.04 times greater for *r2* compared to those during peak storm surge, respectively.

Furthermore, comparison of maximum *Hs* at different stations during normal wave conditions (Fig. 5E and F) revealed wave attenuation of *r1* = 1.58×10^{-3} per meter and *r2* = 1.60×10^{-3} per meter, respectively. In contrast, during Typhoon Muifa, these rates were reduced to *r1* = 1.27×10^{-3} per meter and *r2* = 1.53×10^{-3} per meter. Thus, the attenuation rates during the normal wave conditions were 1.25 times

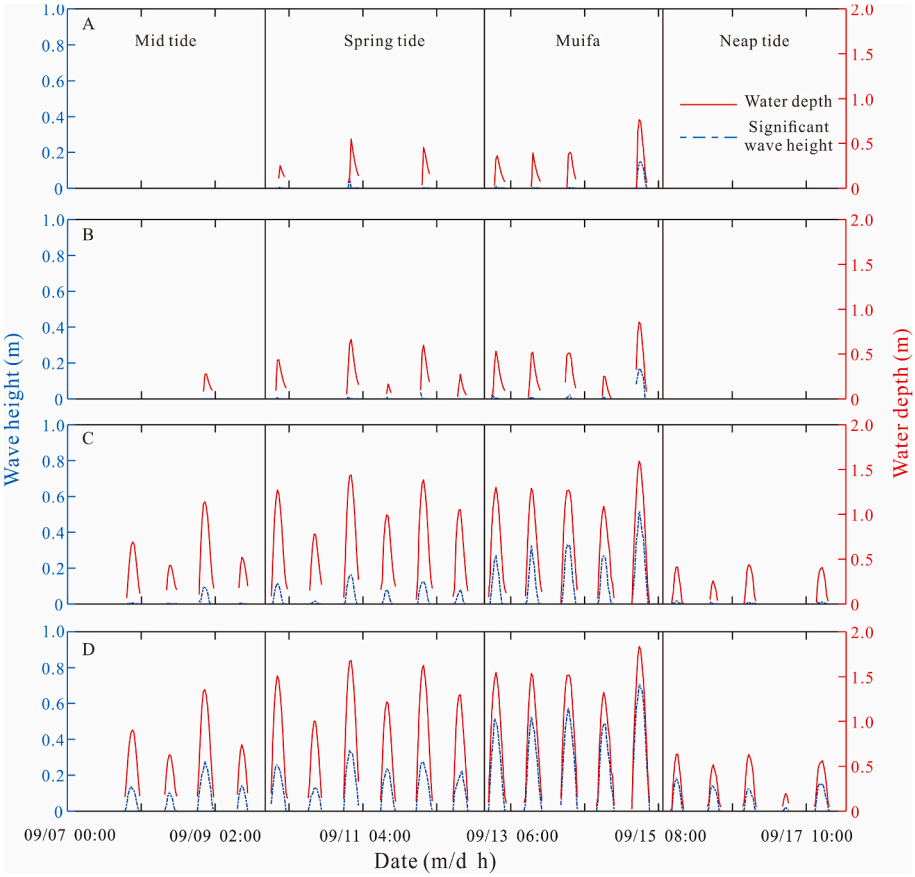

Fig. 4. The figure describes (A) wave height and water depth at SA, (B) wave height and water depth at SB, (C) wave height and water depth at the SC, and (D) wave height and water depth at SD.

greater for *r1* and 1.05 times greater for *r2* compared to those during typhoon Muifa, respectively.

Consequently, typhoon Muifa resulted in elevated water depth and enhanced incident wave heights, with these parameters exhibiting synchronous fluctuations (Fig. 4). As the water depth and incident wave height ascended during Typhoon Muifa, *r1* first increased and then decreased (Figs. 6 and 7). Excessive water depth results in a vertically large distance between the water level and vegetation crest, weakening *r1* and delaying the turning of *r1* (Fig. 7). In detail, *r1* varied when the incident wave height reached 0.15 m during Typhoon Muifa (Fig. 7A–C), while *r1* decreased before the incident wave height reached 0.1 m during normal wave conditions (Fig. 7B–D).

3.4. The drag coefficient under varying conditions

Inundation duration significantly affected the decrease of the drag coefficient (C_D) during the typhoon. The duration of inundation during Muifa was 0.5 h longer than that observed under normal wave conditions in each tide cycle, with deviation exceeding 1.2 h at the marsh front SD and marsh edge (Table 1). As a result, C_D remained low for an extended period during Muifa, substantially diminishing average wave attenuation (Fig. 9). Moreover, the duration in which that *Scirpus mariqueter* was not submerged during Muifa was longer than that of the normal wave conditions, leading to lower C_D values initially (Fig. 9A).

Specifically, during Typhoon Muifa, C_D exhibited a transition from linear increase to an exponential decrease as water depth reached approximately 80% of the height of *Scirpus mariqueter* from the marsh front SD to the marsh edge SC (Fig. 7A). In contrast, from the marsh edge SC to the marsh center SB, the water depth needed to exceed 60% of vegetation height to achieve similar changes (Fig. 9B and 6B). Under normal wave conditions, the transition of C_D and wave attenuation required a greater inundation threshold, with water depth needing to exceed 20% of vegetation height from the marsh front SD to the marsh edge SC (Fig. 9C and 6C). In this context, the growth trend of C_D remained consistent despite changes in inundation state from SC to SB (Fig. 9D and 6D).

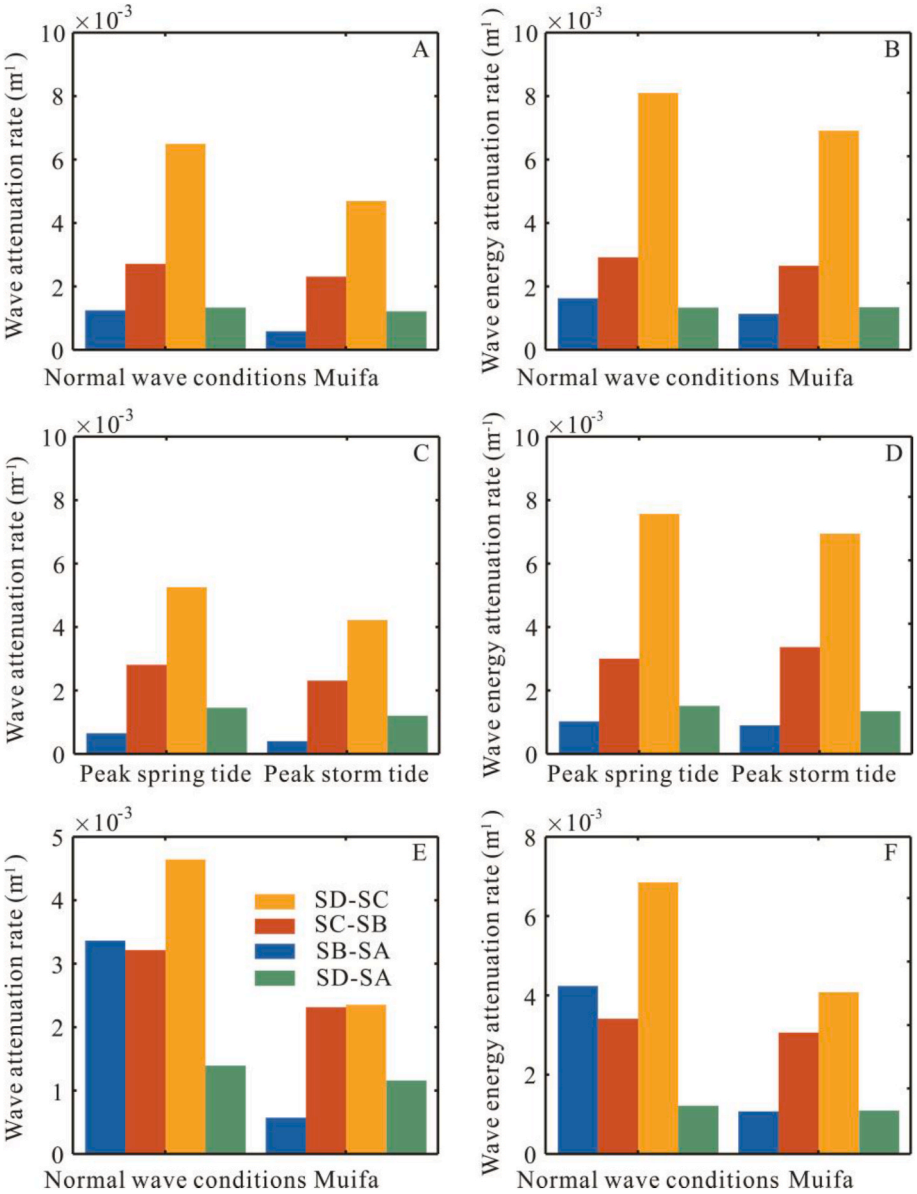

Fig. 5. Wave attenuation rate for (A) average *Hs*, (B) average *E*, (C) peak *Hs*, (D) peak *E*, (E) maximum *Hs*, (F) maximum *E*. Green bars are the rate along the transect from SD to SA, yellow bars are the rate along the transect from SD to SC, blue bars are the rate along the transect from SC to SB, and yellow bars are the rate along the transect from SB to SA.

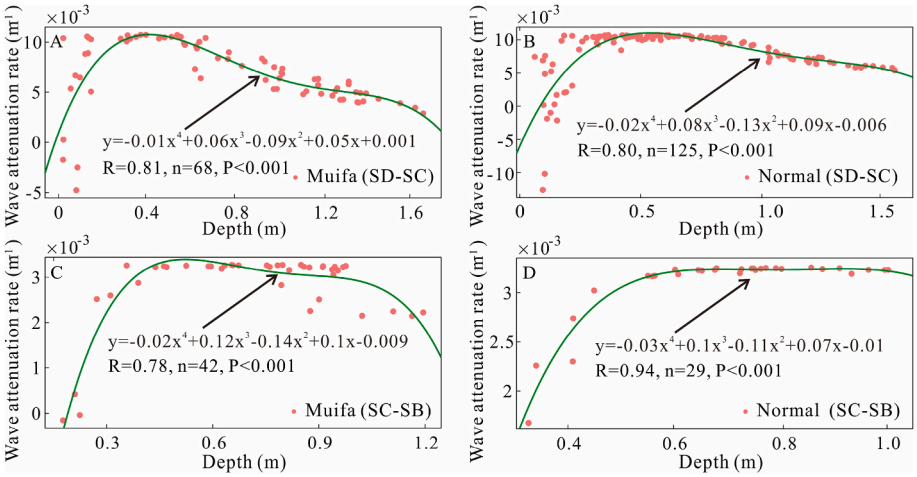

Fig. 6. Correlation between water depth and wave attenuation rate, (A) from SD to SC during Muifa, (B) from SD to SC during normal wave conditions, (C) from SC to SB during Muifa, (D) from SC to SB during normal wave conditions.

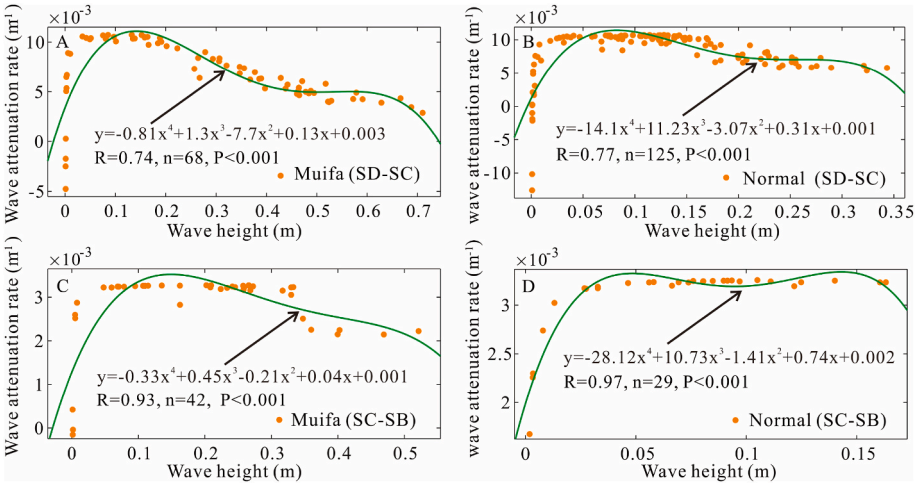

Fig. 7. Correlation between incident wave height and wave attenuation rate, (A) from SD to SC during Muifa; (B) from SD to SC during normal wave conditions, (C) from SC to SB during Muifa, (D) from SC to SB during normal wave conditions.

4. Discussion

4.1. Couplings between water level and wave height

When waves propagated during typhoons, a larger portion of energy was dissipated, owing to the topographic slope and relative water depth (Woodroffe, 2003; Whittaker et al., 2017). In the context of salt marshes, the influence of slope on wave attenuation is relatively minor compared to the effect of the vegetation and relative water depth, particularly when the tidal flat had a minimal gradient (Möller et al., 1999; Willemsen et al., 2020). Given that the gradient observed in this study was only 0.004, the role of slope in wave attenuation was not further examined. However, the differences in incident wave height and water depth emerged as significant factors affecting wave attenuation within the salt marsh (Nepf and Vivoni, 2000; Maza et al., 2015; Rupprecht et al., 2017).

Generally, the larger incident wave height during Typhoon Muifa achieved the same effect during normal wave conditions. Moreover, the increase in incident wave height led to apparent changes in wave attenuation (Willemsen et al., 2020), which advanced the turning of *r1* (Fig. 6). Particularly from SC to SB, the trend of *r1* changed at a water depth of approximately 0.5 m during Typhoon Muifa (Fig. 6C). However, *r1* maintained a level after a water depth of approximately 0.7 m during normal wave conditions (Fig. 6D).

While the rise in water depth hindered wave attenuation during Typhoon Muifa, concomitant increase in incident wave height mitigated the negative impact of water depth on wave attenuation, as observed in Nepf and Vivoni (2000) and Maza et al. (2015) as well. It is important to note that the effects of wave attenuation are not unlimited with increasing water depth and incident wave height. as there are limits to the influence of vegetation on wave attenuation. Therefore, further investigation into the drag coefficient and the inundation state of vegetation is warranted to enhance understanding of wave attenuation process (Möller et al., 2011).

4.2. Inundation state of Scirpus mariqueter on wave attenuation

Salt marsh vegetation dissipates wave energy primarily through the drag coefficient C_D generated by its roots, stems and leaves (Marsooli and Wu, 2014). The magnitude of C_D is influenced by various factors, including vegetation height, density, and submergence state (Massel et al., 1999; Horstman et al., 2014; Foster-Martinez et al., 2018; Devi et al., 2021). In general, the attenuation rate *r1* is related to C_D across different inundation states (Suzuki et al., 2008). Prior to the submergence of *Scirpus mariqueter* (Fig. 8B), both C_D and *r1* increased in response to the rising water levels (Figs. 6 and 9). However, once *Scirpus*

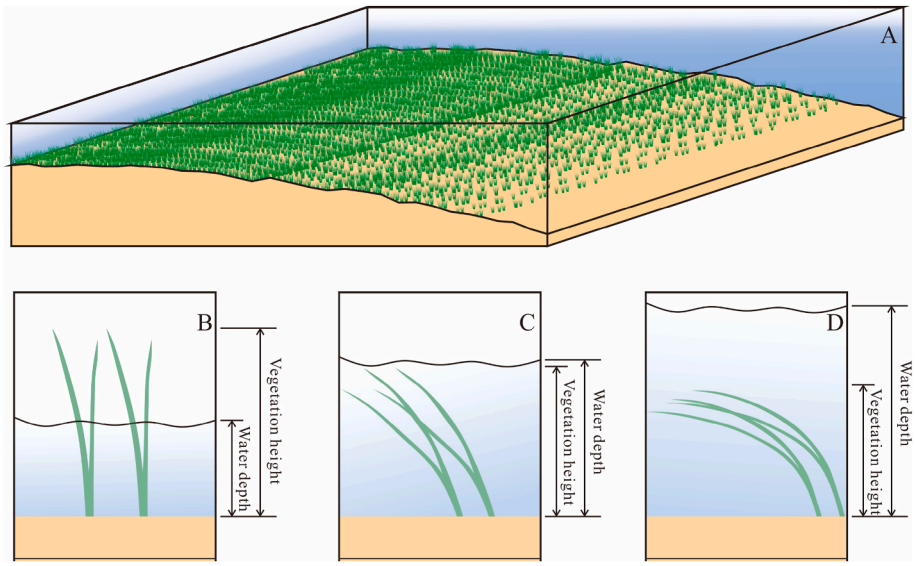

Fig. 8. Inundation state of Scirpus mariqueter: (A) diagram of salt marsh, (B) Scirpus mariqueter before inundation, (C) Scirpus mariqueter submerged, (D) Scirpus mariqueter after inundation.

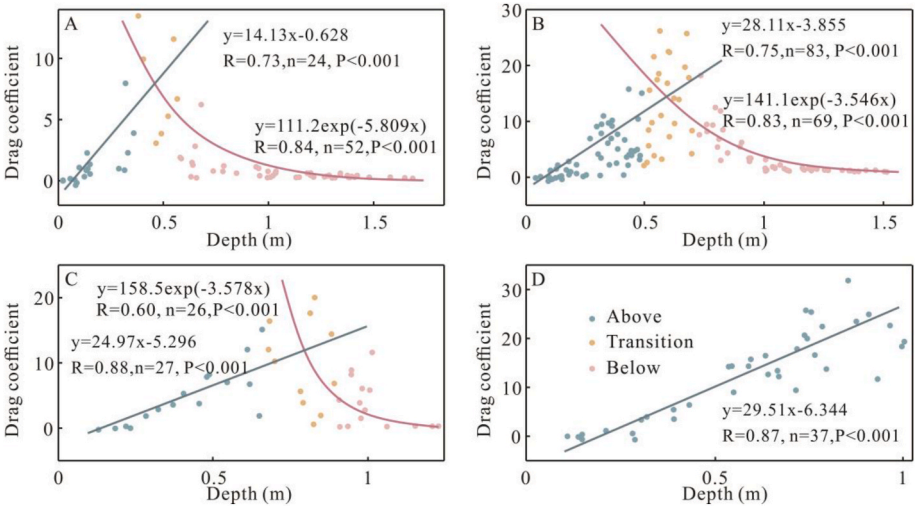

Fig. 9. Correlation between water depth and vegetation resistance, (A) from SD to SC during Muifa; (B) from SD to SC during normal wave conditions, (C) from SC to SB during Muifa, (D) from SC to SB during normal wave conditions.

mariqueter became submerged (Fig. 8C and D), both C_D and *r1* rapidly decreased as water depth continued to increase (Figs. 6 and 9).

Scirpus mariqueter is a flexible vegetation species capable of bending to various degrees, which results in decreases in effective vegetation height as bending increases (Kouwen, 1992). Consequently, the relationship between vegetation height and water depth is not constant across different inundation stages (Fig. 8). Under equivalent submergence conditions, spatial variations in C_D and *r1* are influenced by vegetation density (Suzuki et al., 2008). Near the inner marsh site SA, increased vegetation correlated with higher C_D at the same vegetation height (Fig. 6). During Typhoon Muifa, the same C_D necessitated greater vegetation density and height due to significantly increased incident wave heights (Fig. 7).

The relationship between C_D under varying inundation states and *r1* has been established in previous studies (Morison et al., 1950; Zhou et al., 2022). Notably, *r1* increased exponentially with the increase in C_D (Fig. 10). When water depth is insufficient to fully submerge the vegetation, both C_D and *r1* are restricted due to the limited water flow through the vegetation (Nepf and Vivoni, 2000). When the water depth was excessive and beyond the top of vegetation, C_D also decreased (Möller et al., 2011). Moreover, compared to the condition that the *Scirpus mariqueter* was semi-submerged, C_D was lower for a longer time when the *Scirpus mariqueter* was submerged, which resulted in a low *r1* for some time (Figs. 9 and 10). This is why *r1* during typhoons is lower than during normal wave conditions, as the water level exceeds the top of the vegetation for a longer duration during typhoons.

4.3. Wave attenuation effect of different salt marshes during the typhoon

Wave attenuation during typhoons is influenced by the vegetation types present in intertidal zones. Möller et al. (2011) reported that low salt marshes dominated by *Scirpus mariqueter*, exhibited relatively low wave attenuation rates, with values of 0.09%/m at the vegetation boundary and 0.13%/m within the salt marsh itself. In contrast, mudflats showed even lower wave attenuation rates of only 0.05%/m. A significant increase in wave attenuation rates was observed when transitioning from mudflats to areas dominated by *Scirpus mariqueter*, reaching up to 1.10%/m (Yang et al., 2008). Further transitions to zones

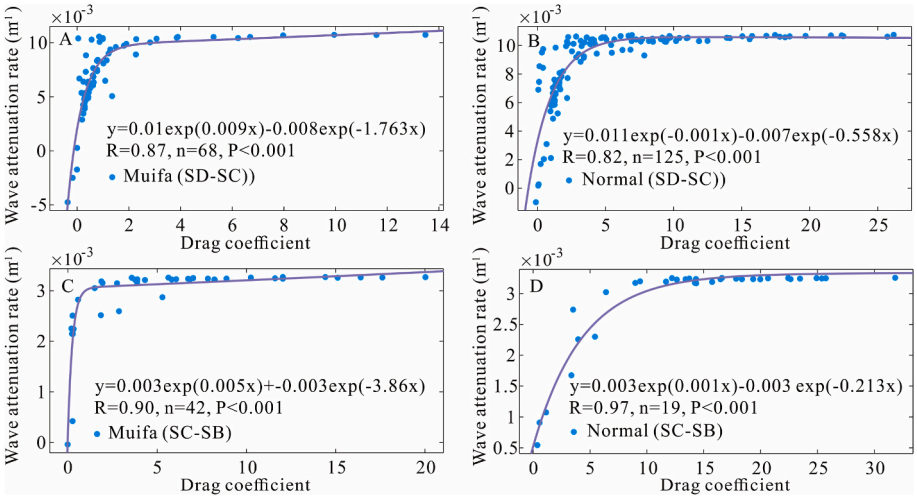

Fig. 10. Correlation between vegetation resistance and wave attenuation rate, (A) from SD to SC during Muifa; (B) from SD to SC during normal wave conditions, (C) from SC to SB during Muifa, (D) from SC to SB during normal wave conditions.

dominated by Spartina alterniflora resulted in even higher attenuation rates, with values soaring up to 2.74%/m (Yang et al., 2012). Notably, Spartina alterniflora salt marshes exhibited attenuation rates of 1.34%/m and 1.49%/m at SC during storm surge events (Paquier et al., 2017; Zhang et al., 2020b).

When comparing different vegetation types, rigid vegetation species such as Bulrushes were found to dissipate waves more effectively than both *Scirpus mariqueter* and Spartina alterniflora (Van Veelen et al., 2020). Zhang et al. (2022a) reported wave attenuation rates of 2.15%/m at the edge of Bulrush salt marshes, reducing to 1.00%/m within the salt marsh. Mangroves, known for their coastal protection capabilities, exhibited attenuation rates of 0.84%/m and 0.60%/m at their external and internal zones, respectively (Zhang et al., 2022b). In the present study, *Scirpus mariqueter* demonstrated lower rates of 0.24%/m and 0.23%/m at the boundary and internal zones, respectively, and only 0.05%/m at deeper regions during Typhoon Muifa (Table 2).

Considering the wave attenuation capabilities of various vegetation types (Fig. 11), it is evident that *Bulrush* salt marshes exhibited the highest attenuation rates, achieving a 60% reduction in wave height reduction at 50 m from SC and a remarkable 98% reduction at a distance of 200 m from the edge (Yang et al., 2012; Zhang et al., 2022a). In comparison, *Spartina alterniflora* and mangrove salt marshes achieved similar attenuation rates, with 98% wave height reduction at a distance of 400 m from SC. These findings suggest that a Bulrush salt marsh covering only one-third the width of a *Scirpus mariqueter* salt marsh would achieve similar wave attenuation ratios. Furthermore, planting a 200 m-wide Bulrush salt marsh or a 300 m-wide Spartina alterniflora salt marsh along the shore would result in substantial wave attenuation.

5. Conclusion

Salt marsh vegetation has attracted worldwide attention for its capability to protect wetland ecosystems. This study investigated wave attenuation in salt marshes under varying wave conditions through hydrological observations conducted north of Chongming Dongtan. The key findings are as follows.

1. Wave attenuation within the *Scirpus mariqueter* salt marsh exhibited a gradual decrease landward Under normal wave conditions, the marsh demonstrated a significant capacity for wave attenuation, with significant wave height declined by 98%. However, during Typhoon Muifa, the average significant wave height declined by 92%.

Table 2
The significant wave height and wave attenuation of different species in different studies.

Distance (m)	Vegetation species	Hs (m)	Attenuation (%/m)	Reference
0	*Mudflat*	0.36		Yang et al. (2008)
185	*Mudflat*	0.33	0.05	
201.5	*Scirpus mariquter*	0.27	1.1	
215	*Spartina alterniflora*	0.17	2.74	
0	*Sandflat*	0.67		Möller et al., 2011
220	*Low salt marsh*	0.56	0.07	
460	*Low salt marsh*	0.38	0.13	
0	*Mudflat*	0.48		Yang et al. (2012)
27.5	*Scirpus mariquter*	0.33	0.55	
68.5	*Spartina alterniflora*	0.14	1.37	
0	*Mudflat*	0.34		Paquier et al. (2017)
22	*Spartina alterniflora*	0.24	1.34	
48	*Spartina alterniflora*	0.15	1.44	
127	*Spartina alterniflora*	0.07	0.68	
0	*Mudflat*	0.67		
10	*Spartina alterniflora*	0.57	1.49	
0	*Mudflat*	0.57		Zhang et al. (2022a)
140	*Mudflat*	0.28	0.36	
187	*Mangroves*	0.17	0.84	
304	*Mangroves*	0.05	0.6	
0	*Mudflat*	0.26		Zhang et al. (2022a)
25	*Bulrush*	0.12	2.15	
50	*Bulrush*	0.09	1	
0	*Mudflat*	0.71		This study
113	*Scirpus mariquter*	0.52	0.24	
405	*Scirpus mariquter*	0.17	0.23	
626	*Scirpus mariquter*	0.15	0.05	

2. Wave attenuation was primarily influenced by the effects of the typhoon and the inundation state of the salt marsh. While Typhoon Muifa increased the incident wave heights, the significant surge in water levels created a greater distance between the vegetation crest and the water level, thereby diminishing the wave attenuation capacity of *Scirpus mariqueter*. Meanwhile, wave attenuation increased exponentially with increasing drag coefficients C_D, which were influenced by the interplay of the inundation state and vegetation density.

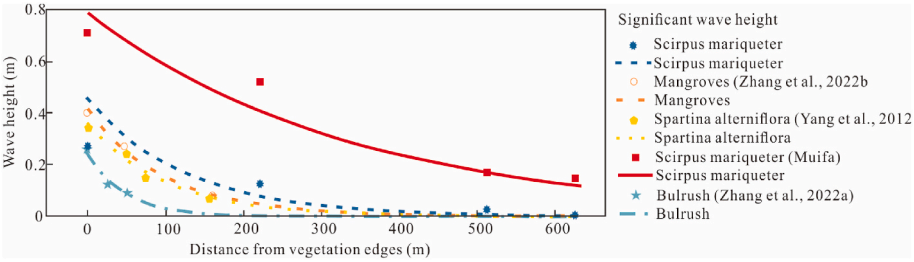

Fig. 11. Wave dissipation state of different vegetation types during the typhoon.

3. During typhoon events, wave attenuation in the *Scirpus mariqueter* salt marsh was predominantly constrained by vegetation height and width. Remarkably, a *Bulrush* salt marsh covering only one-third of the width of the *Scirpus mariqueter* salt marsh achieved a comparable wave attenuation ratio. Therefore, it is recommended to consider the establishment of a 200 m-wide *Bulrush* salt marsh on the inner side of the study area as an effective defensive measure against typhoon impacts.

CRediT authorship contribution statement

Ming Shi: Writing – original draft, Methodology, Data curation. **Zhijun Dai:** Construction, Writing – origina draft, review & editing, Supervision, Methodology, Funding acquisition, Formal analysis. **Jiejun Luo:** Methodology, Investigation, Data curation. **Jie Wang:** Data curation. **Wenhong Pang:** Formal analysis, Data curation. **Xixing Liang:** Data curation. **Jinping Cheng:** Writing – review & editing.

Declaration of competing interest

The authors declare that there are no conflicts of interest regarding the submitted paper of "***Wave attenuation over a Scirpus mariqueter salt marsh during Typhoon Muifa***".

Acknowledgments

This study was supported financially by National Key R&D Program of China (2023YFE0121200), National Natural Science Key Foundation of China (U2040202), and Shanghai International Science and Technology Cooperation Fund Project (23230713800). Thanks to the three reviewers for their suggestions.

Data availability

Data will be made available on request.

References

Augustin, L.N., Irish, J.L., Lynett, P., 2013. Laboratory and numerical studies of wave damping by emergent and near-emergent wetland vegetation. Coastal Engineering 56, 332–340.
Battjes, J.A., Janssen, J.P.F.M., 1978. Energy loss and set-up due to breaking of random waves. Coast. Eng 1978, 569–587.
Beena, M.J., Kiran, G.S., Subba, R., 2019. Laboratory investigations of wave attenuation by simulated vegetation of varying densities. ISH Journal of Hydraulic Engineering 25 (2), 203–213.
Bouma, T.J., de Vries, M.B., Low, E., Peralta, G., Tánczos, I.C., van de Koppel, J., Herman, P.M.J., 2005. Trade-offs related to ecosystem engineering: a case study on stiffness of emerging macrophytes. Ecology 86, 2187–2199.
Bretschneider, C.L., Reid, R.O., 1954. Modification of wave-height due to bottom friction, percolation and refraction. Beach Erosion Board, Corps of Engineers. Tech. Memo. 45, 1–36.
Bryant, E.A., 1979. Comparison of computed and observed breaker wave heights. Coastal Engineering 3, 39–50.
Chen, Q., Zhao, H., 2012. Theoretical models for wave energy dissipation caused by vegetation. J. Eng. Mech. 138 (2), 221–229.
Chong, Z.T., Zhang, M., Wen, J.H., Wang, L.Y., Jeremy, B., Stanley, N., Dai, Z.J., 2021. Coastal protection using building with nature concept: a case study from Chongming Dongtan Shoal, China. Acta Oceanol. Sin 40, 152–166.
Deegan, L.A., Johnson, D.S., Warren, R.S., Peterson, B.J., Fleeger, J.W., Fagherazzi, S., Wollheim, W.M., 2012. Coastal eutrophication as a driver of salt marsh loss. Nature 490, 388–392.
Devi, C., Jairaj, P.G., Balan, K., 2021. Laboratory investigations on wave attenuation characteristics of Rhizophora Mucronata poir using physical models with bottom friction. Environ. Fluid Mech. 21 (2), 361–381.
Foster-Martinez, M.R., Lacy, J.R., Ferner, M.C., Variano, E.A., 2018. Wave attenuation across a tidal marsh in San Francisco bay. Coast. Eng 136, 26–40.
Garzon, J.L., Miesse, T., Ferreira, C.M., 2019. Field-based numerical model investigation of wave propagation across marshes in the Chesapeake Bay under storm conditions. Coastal Engineering 146, 32–46.
Gorenc, S., Kostaschuk, R., Chen, Z., 2004. Spatial variations in heavy metals on tidal flats in the Yangtze Estuary, China. Environmental geology 45, 1101–1108.
Gracia, A., Rangel-Buitrago, N., Oakley, J.A., Williams, A.T., 2018. Use of ecosystems in coastal erosion management. Ocean Coast. Manag 156, 277–289.
Heuner, M., Silinski, A., Schoelynck, J., Bouma, T.J., Puijalon, S., Troch, P., Fuchs, E., Schroder, B., Schroder, U., Meire, P., Temmerman, S., 2017. Ecosystem engineering by plants on wave-exposed intertidal flats is governed by relationships between effect and response traits. PLoS One 10, e0138086.
Holthuijsen, L.H., 2007. Waves in Oceanic and Coastal Waters. Cambridge University Press, Cambridge.
Horstman, E.M., Dohmen-Janssen, C.M., Narra, P.M.F., van den Berg, N.J.F., Siemerink, M., Hulscher, S.J.M.H., 2014. Wave attenuation in mangroves: a quantitative approach to field observations. Coast. Eng 94, 47–62. https://doi.org/10.1016/j.coastaleng.2014.08.005.
Jadhav, R.S., Chen, Q., Smith, J.M., 2013. Spectral distribution of wave energy dissipation by salt marsh vegetation. Coastal Engineering 77, 99–107.
Kearney, M.S., Stevenson, J.C., 1991. Island land loss and marsh vertical accretion rate evidence for historical sea - level changes in Chesapeake Bay. J. Coast Res. 1991, 403–415.
Kirwan, M.L., Megonigal, J.P., 2013. Tidal wetland stability in the face of human impacts and sea-level rise. Nature 504, 53–60.
Kobayashi, N., Raichle, A.W., Asano, T., 1993. Wave attenuation by vegetation. Journal of waterway, port. Coastal and Ocean Engineering 199, 30–48.
Kouwen, N., 1992. Modern approach to design of grassed channels. Journal of Irrigation and Drainage Engineering-asce 118, 733–743.
Latapy, A., Héquette, A., Pouvreau, N., Weber, N., Robin-Chanteloup, J., 2019. Mesoscale morphological changes of nearshore sand banks since the early 19th century, and their influence on coastal dynamics, northern France. J. Mar. Sci. Eng. 7, 73.
Leonardi, N., 2021. The barriers of Venice. Nat. Geosci. 14, 881–882.
Lou, Y.Y., Dai, Z.J., Long, C.Q., Dong, H., Wei, W., Ge, Z.P., 2022. Image-based machine learning for monitoring the dynamics of the largest salt marsh in the Yangtze River Delta. J. Hydrol. 608.
Luhar, M., Coutu, S., Imfantes, E., Fox, S., Nepf, H., 2010. Wave-induced velocities inside a model seagrass bed. J. Geophys. Res.: Oceans 115, C12005.
Ma, Y., Zhu, L., Peng, Z., Xue, L., Zhao, W., Li, T., Lin, S., Bouma, T.J., Hofland, B., Dong, C., Li, X., 2023. Wave attenuation by flattened vegetation (Scirpus mariqueter). Front. Mar. Sci. 10, 1106070.
Mariotti, G., Fagherazzi, S., 2010. A numerical model for the coupled long-term evolution of salt marshes and tidal flats. J. Geophys. Res.: Earth Surf. 115, 1–15.
Marsooli, R., Wu, W., 2014. Numerical investigation of wave attenuation by vegetation using a 3D RANS model. Adv. Water Resour. 74, 245–257.
Marsooli, R., Orton, P.M., Mellor, G., Georgas, N., Blumberg, A.F., 2017. A coupled circulation–wave model for numerical simulation of storm tides and waves. J. Atmos. Oceanic Technol. 34, 1449–1467.
Massel, S.R., Furukawa, K., Brinkman, R.M., 1999. Surface wave propagation in mangrove forests. Fluid. Dyn. Res. 24, 219–249.
Maza, M., Lara, J.L., Losada, I.J., Ondiviela, B., Trinogga, J., Bouma, T.J., 2015. Large-scale 3-Dexperiments of wave and current interaction with real vegetation. Part 2: experimental analysis. Coastal Engineering 106, 73–86.
Mazda, Y., Magi, M., Kogo, M., Hong, P.N., 1997. Mangroves as a coastal protection from waves in the Tong King delta. Vietnam. Mangroves&Salt Marshes 1, 127–135.
Mazda, Y., Magi, M., Ikeda, Y., Kurikawa, T., Asano, T., 2006. Wave reduction in a mangrove forest dominated by Sonneratiasp. Wetl. Ecol. Manag. 14 (4), 365–378.
Mei, W., Xie, S.P., 2016. Intensification of landfalling typhoons over the northwest Pacific since the late 1970s. Nat. Geosci. 9, 753–757.

Mendez, F.J., Losada, I.J., 2004. An empirical model to estimate the propagation of random breaking and nonbreaking waves over vegetation fields. Coastal Engineering 51, 103–118.
Mi, J., Zhang, M., Zhu, Z.C., Vuik, V., Wen, J.H., Gao, H.K., Bouma, T.J., 2022. Morphological wave attenuation of the nature-based flood defense: a case study from Chongming Dongtan Shoal, China. Sci. Total Environ. 831, 154813.
Möller, I., Spencer, T., French, J.R., Leggett, D.J., Dixon, M., 1999. Wave transformation over salt marshes: a field and numerical modelling study from North Norfolk, England. Estuarine,. Coastal and Shelf Science 49, 411–426.
Möller, I., Mantilla-Contreras, J., Spencer, T., Hayes, A., 2011. Micro-tidal coastal reed beds: hydro-morphological insights and observations on wave transformation from the southern Baltic Sea. Estuar. Coast Shelf Sci. 92, 424–436.
Möller, I., Kudella, M., Rupprecht, F., Spencer, T., Paul, M., van Wesenbeeck, B.K., Wolters, G., Jensen, K., Bouma, T.J., Miranda-lange, M., Schimmels, S., 2014. Wave attenuation over coastal salt marshes under storm surge conditions. Nature Geosci 7, 727–731.
Morison, J.R., Johnson, J.W., Schaaf, S.A., 1950. The force exerted by surface waves on piles. J. Petrol. Technol. 2, 149–154.
Nepf, H.M., Vivoni, E.R., 2000. Flow structure in depth-limited, vegetated flow. Journal of Geophysical Research Oceans 105, 28547–28557.
Neumeier, U., Amos, C.L., 2006. The influence of vegetation on turbulence and flow velocities in European salt-marshes. Sedimentology 53, 259–277.
Nordio, G., Fagherazzi, S., 2022. Storm surge and tidal dissipation in deltaic wetlands bordering a main channel. J. Geophys. Res.: Oceans 127 (3), e2021JC017655.
Paquier, A.E., Haddad, J., Lawler, S., Ferreira, M.C., 2017. Quantification of the attenuation of storm surge components by a coastal wetland of the US mid atlantic. Estuar. Coast 40, 930–946.
Paul, M., Bouma, T.J., Amos, C.L., 2012. Wave attenuation by submerged vegetation: combining the effect of organism traits and tidal current. Mar. Ecol. Prog. Ser. 444, 31–41.
Paul, M., Rupprecht, F., Moller, I., et al., 2016. Plant stiffness and biomass as drivers for drag forces under extreme wave loading: a flume study on mimics. Coastal Engineering 117, 70–78.
Puijalon, S., Bouma, T.J., Douady, C.J., van Groenendael, J., Anten, N.P.R., Martel, E., Bornette, G., 2011. Plant resistance to mechanical stress: evidence of an avoidance–tolerance trade-off. New Phytol. 191, 1141–1149.
Riffe, K.C., Hederson, S.M., Mullarney, J.C., 2011. Wave dissipation by flexible vegetation. Geophys. Res. Lett. 38, L18607.
Rupprecht, F., Moller, I., Paul, M., Kudella, M., Spencer, T., van Wesenbeeck, B.K., Wolters, G., Jensen, K., Bouma, T.J., Miranda-Lange, M., Schimmels, S., 2017. Vegetation-wave interactions in salt marshes under storm surge conditions. Ecol. Eng. 100, 301–315.
Silinski, A., Heuner, M., Schoelynck, J., Puijalon, S., Schröder, U., Fuchs, E., Troch, P., Bouma, T.J., Meire, P., Temmerman, S., 2015. Effects of wind waves versus ship waves on tidal marsh plants: a flume study on different life stages of scirpus maritimus. PLoS One 10, e0118687.
Smith, J.M., Bryat, M.A., Wamsley, T.V., 2016. Wetland buffers: numerical modeling of wave dissipation by vegetation. Earth Surf. Process. Landforms 41 (6), 847–854.
Spencer, T., Möller, I., Rupprecht, F., Bouma, T.J., van Wesenbeeck, B.K., Kudella, M., Paul, M., Jensen, K., Wolters, G., Miranda-Lange, M., Schimmels, S., 2016. Salt marsh surface survives true-to-scale simulated storm surges. Earth Surf. Process. Landforms 41, 543–552.
Stark, J., Van Oyen, T., Meire, P., Temmerman, S., 2015. Observations of tidal and storm surge attenuation in a large tidal marsh. Limnol. Oceanogr. 60 (4), 1371–1381.
Suzuki, T., Dijkstra, J., Stive, M.J.F., 2008. Wave dissipation on a vegetated salt marsh. In: Proceedings of the 31st ICCE. Hamburg, Germany, pp. 331–343.
Temmerman, S., Bouma, T.J., Govers, G., Wang, Z.B., De Vries, M.B., Herman, P.M.J., 2005. Impact of vegetation on flow routing and sedimentation patterns: three-dimensional modeling for a tidal marsh. J. Geophys. Res. 110, F04019.
Temmerman, S., Meire, P., Bouma, T.J., Herman, P.M.J., Ysebaert, T., De Vriend, H.J., 2013. Ecosystem-based coastal defence in the face of global change. Nature 504, 79–83.
Van Loon-Steensma, J.M., 2015. Salt marshes to adapt the flood defences along the Dutch Wadden Sea coast. Mitig. Adapt. Strateg. Glob. Change 20 (6), 929–948.
Van Proosdij, D., Ollerhead, J., Davidson-arnott, R.G.D., 2000. Controls on Suspended Sediment Deposition over Single Tidal Cycles in a Macrotidal Saltmarsh, Bay of Fundy, Canada. Geological Society, London, vol. 175. Special Publications, pp. 43–57.
Van Proosdij, D., Davidson-arnott, R.G.D., Ollerhead, J., 2006. Controls on spatial patterns of sediment deposition across a macro-tidal salt marsh surface over single tidal cycles. Estuarine. Coastal and Shelf Science 69 (1–2), 64–86.
Van Veelen, T.J., Fairchild, T.P., Reeve, D.E., Karunarathna, H., 2020. Experimental study on vegetation fexibility as control parameter for wave damping and velocity structure. Coast. Eng 157, 103648.
Wei, W., Dai, Z.J., Pang, W.H., et al., 2022. Frequency-dependent wave damping by tidal wetlands under storm conditions. J. Hydrol. 613, 128415.
Whittaker, C.N., Fitzgerald, C.J., Raby, A.C., Taylor, P.H., Orszaghova, J., Borthwick, A. G.L., 2017. Optimisation of focused wave group runup on a plane beach. Coastal Engineering 121, 44–55.
Willemsen, P.W.J.M., Borsje, B.W., Vuik, V., Bouma, T.J., Hulscher, S.J.M.H., 2020. Field-based decadal wave attenuating capacity of combined tidal flats and salt marshes. Coastal Engineering 156, 103628.
Woodroffe, C.D., 2003. Coasts: Form, Processes and Evolution. Cambridge University Press, Cambridge.
Xu, Y., Esposito, C.R., Burgos, M.B., Nepf, H.M., 2022. Competing effects of vegetation on sedimentation in deltaic marshes. Nat. Commun. 13, 4641.
Yang, S.L., Li, H., Ysebaert, T., et al., 2008. Spatial and temporal variations in sediment grain size in tidal wetlands, Yangtze Delta: on therole of physical and biotic controls. Estuarine. Coastal and Shelf Science 77, 657–671.
Yang, S.L., Shi, B.W., Bouma, T.J., Ysebaert, T., Luo, X.X., 2012. Wave attenuation at a salt marsh margin: a case study of an exposed coast on the yangtze estuary. Estuar. Coast 35, 169–182.
Young, I.R., Gorman, R.M., 1995. Measurements of the evolution of ocean wave spectra due to bottom friction. J. Geophys. Res. 100 (C6), 10987–11004.
Zhang, X., Xiao, X., Wang, X., Xu, X., Chen, B., Wang, J., Ma, J., Zhao, B., Li, B., 2020a. Quantifying expansion and removal of spartina alterniflora on Chongming island, China, using time series landsat images during 1995–2018. Remote Sens. Environ. Times 247, 111916.
Zhang, W., et al., 2020b. The role of seasonal vegetation properties in determining the wave attenuation capacity of coastal marshes: implications for building natural defenses. Ecol. Eng. 175, 106494.
Zhang, W., Ge, Z.M., Li, S.H., Tan, L.S., Zhou, K., Li, Y.L., Xie, L.N., Dai, Z.J., 2022a. The role of seasonal vegetation properties in determining the wave attenuation capacity of coastal marshes: implications for building natural defenses. Ecol. Eng. 175.
Zhang, X., Lin, P., Chen, X., 2022b. Coastal protection by planted mangrove forest during typhoon mangkhut. J. Mar. Sci. Eng. 10, 1288.
Zhou, X., Dai, Z., Pang, W., Wang, J., Long, C., 2022. Wave attenuation over mangroves in the nanliu delta, China. Front. Mar. Sci. 9, 874818.